The prognostic value of dynamic contrast-enhanced MRI contrast agent transfer constant Ktrans in cervical cancer is explained by plasma flow rather than vessel permeability

FULL PAPER

BJC

British Journal of Cancer (2017) 116, 1436–1443 | doi: 10.1038/bjc.2017.121

Keywords: cervix cancer; DCE-MRI; prognostic biomarker; plasma flow; K^{trans}; permeability surface-area product

The prognostic value of dynamic contrast-enhanced MRI contrast agent transfer constant K^{trans} in cervical cancer is explained by plasma flow rather than vessel permeability

Ben R Dickie*[,1,2], Chris J Rose[3], Lucy E Kershaw[1,2], Stephanie B Withey[4], Bernadette M Carrington[5], Susan E Davidson[5], Gillian Hutchison[6] and Catharine M L West[1]

[1]*Division of Molecular and Clinical Cancer Sciences, The University of Manchester, Manchester Academic Health Science Centre, Manchester M20 4BX, UK;* [2]*Christie Medical Physics and Engineering, The Christie NHS Foundation Trust, Manchester M20 4BX, UK;* [3]*Centre for Imaging Sciences, Division of Informatics, Imaging, and Data Sciences, The University of Manchester, Manchester Academic Health Science Centre, Manchester M13 9PG, UK;* [4]*RRPPS, University Hospitals Birmingham NHS Foundation Trust, Birmingham B30 3HP, UK;* [5]*Department of Diagnostic Radiology, The Christie NHS Foundation Trust, Manchester M20 4BX, UK and* [6]*Department of Radiology, Royal Bolton NHS Foundation Trust, Farnworth BL4 0JR, UK*

Background: The microvascular contrast agent transfer constant K^{trans} has shown prognostic value in cervical cancer patients treated with chemoradiotherapy. This study aims to determine whether this is explained by the contribution to K^{trans} of plasma flow (F_p), vessel permeability surface-area product (*PS*), or a combination of both.

Methods: Pre-treatment dynamic contrast-enhanced MRI (DCE-MRI) data from 36 patients were analysed using the two-compartment exchange model. Estimates of F_p, *PS*, K^{trans}, and fractional plasma and interstitial volumes (v_p and v_e) were made and used in univariate and multivariate survival analyses adjusting for clinicopathologic variables tumour stage, nodal status, histological subtype, patient age, tumour volume, and treatment type (chemoradiotherapy *vs* radiotherapy alone).

Results: In univariate analyses, F_p (HR = 0.25, $P = 0.0095$) and K^{trans} (HR = 0.20, $P = 0.032$) were significantly associated with disease-free survival while *PS*, v_p and v_e were not. In multivariate analyses adjusting for clinicopathologic variables, F_p and K^{trans} significantly increased the accuracy of survival predictions ($P = 0.0089$).

Conclusions: The prognostic value of K^{trans} in cervical cancer patients treated with chemoradiotherapy is explained by microvascular plasma flow (F_p) rather than vessel permeability surface-area product (*PS*).

Dynamic contrast-enhanced MRI (DCE-MRI) has been extensively used to study the relationship between pre-treatment microvascular function and treatment outcome in locally advanced cervix cancer (Mayr *et al*, 1996, 2010; Semple *et al*, 2009; Yuh *et al*, 2009; Zahra *et al*, 2009; Andersen *et al*, 2013). Greater uptake of contrast agent by tumour tissue measured using MRI signal enhancement

*Correspondence: Dr BR Dickie; E-mail: ben.dickie@manchester.ac.uk

Received 17 March 2017; revised 6 April 2017; accepted 6 April 2017; published online 27 April 2017

or quantitative model-based parameters such as K^{trans} (Tofts *et al*, 1999), has been shown to be a positive prognostic factor (Mayr *et al*, 1996, 2010; Semple *et al*, 2009; Yuh *et al*, 2009; Zahra *et al*, 2009; Andersen *et al*, 2013). Increased uptake of contrast agent before treatment may reflect a tumour that is better oxygenated (improving radio-sensitivity) and more easily infiltrated with chemotherapy agents via the vasculature, thus improving the chances of treatment success and reducing the risk of recurrence.

Uptake of contrast agent into tumour tissue depends on a number of microvascular factors. For example, a measurement of K^{trans} depends on the delivery of contrast agent to the capillary bed (plasma flow; F_p) and exchange flow of contrast agent across the vessel wall (as measured by the permeability surface-area product; *PS*) (Tofts *et al*, 1999; Sourbron and Buckley, 2011). It is therefore currently unknown whether perfusion, or vessel permeability surface area product, or both are responsible for the observed relationship between K^{trans} and the survival of cervical cancer patients treated with chemoradiotherapy. Knowledge of this may open new avenues for targeted treatments and allow better stratification of patients into distinct prognostic groups.

Improvements in the temporal resolution of DCE-MRI sequences (Stollberger and Fazekas, 2004) have facilitated independent measurement of plasma flow (F_p) and permeability surface area product (*PS*) using the two-compartment exchange (2CXM; Brix *et al*, 2004) and adiabatic approximation to the tissue homogeneity models (St Lawrence and Lee, 1998). This paper describes a prospective study in which the two-compartment exchange model is used to independently measure F_p and *PS* in 36 patients with locally advanced cervix cancer treated with chemoradiotherapy. It was hypothesised that survival is limited by the delivery of oxygen and chemotherapy via plasma flow rather than vessel permeability surface area product, and that plasma flow is therefore a more accurate prognostic factor than *PS* and K^{trans}. Data and software for performing all analyses described in this paper are available at https://github.com/MRdep/Predicting-Survival-In-Cervical-Cancer-using-DCE-MRI (Dickie, 2017).

MATERIALS AND METHODS

Study outline. The study was prospective and received local research ethics committee approval from the South Manchester Research Ethics Committee (Ref: 05/Q1403/28). Eligible patients had biopsy proven locally advanced carcinoma of the cervix and planned treatment with radical concurrent chemoradiotherapy, followed by either a low-dose rate brachytherapy or external beam radiotherapy boost. Exclusion criteria were age <18 years and contraindication for MRI.

A total of 40 patients were recruited at a single centre between July 2005 and March 2010. All patients gave written informed consent before involvement in the study. Patients received DCE-MRI $\sim$1 week before the first fraction of radiotherapy and received standard follow-up for detection of recurrence. Survival analysis was undertaken to infer the prognostic effect and predictive value of DCE-MRI and clinicopathologic variables. DCE-MRI data from four patients could not be analysed, leaving a total of 36 patients for inclusion in survival analyses. Supplementary Figure 1 shows a CONSORT diagram for the study (Moher *et al*, 2001).

Treatment. Each patient received external beam radiotherapy (EBRT) to the whole pelvis (up to L4) with a dose of 40–45 Gy in 20 fractions. Cisplatin chemotherapy was administered concurrently in 2–4 cycles where tolerated. Brachytherapy boosts were administered in one fraction following EBRT (20–32 Gy). External beam radiotherapy boosts were delivered in 8–10 fractions (20–32 Gy).

MRI protocol. MRI was performed on a 1.5 T Siemens Magnetom Avanto scanner (Siemens Medical Solutions, Erlangen, Germany). MRI acquisition parameters have been described in detail previously (Donaldson *et al*, 2010). Briefly, a high spatial resolution 2D T_2-weighted turbo spin echo scan (FOV $= 240 \times 320\,mm^2$, 16×5 mm slices, voxel size $= 0.63 \times 0.63\,mm^2$, TR $= 5390$ ms, TE $= 118$ ms, NSA $= 2$) was acquired for defining tumour regions of interest (ROIs). A 3D T_1-weighted spoiled gradient-recalled echo (SPGR) volumetric interpolated breath-hold examination sequence, with the same field of view as T_2-weighted scans but lower spatial resolution (voxel size $= 2.5 \times 2.5 \times 5\,mm^3$, TR/TE $= 5.6/1.08$ ms, SENSE factor $= 2$), was used for pre-contrast T_1 mapping (flip angles: 5, 10, and 35°, NSA $= 10$) and dynamic imaging (flip angle: 25°, NSA $= 1$). Pre-contrast T_1 was used to convert dynamic signal intensity into contrast agent concentration for tracer kinetic modelling. Dynamic imaging was performed with a temporal resolution of 3 s to facilitate measurement of plasma flow (F_p) and permeability surface-area product (*PS*) using the 2CXM. A total of 80 dynamic volumes were acquired for a total DCE-MRI acquisition time of 4 min. A bolus of 0.1 mmol kg^{-1} gadopentetate dimeglumine (Gd-DTPA; Magnevist, Bayer-Schering Pharma AG, Berlin, Germany) was administered 15 s into the dynamic scan at 4 ml s^{-1} using a power injector through a cannula placed in the antecubital vein, followed by a 20 ml saline flush. Imaging was performed in the sagittal plane with the read encoding direction aligned along the superior–inferior direction to minimise inflow enhancement effects (Donaldson *et al*, 2010).

DCE-MRI analysis. Tumour ROIs were delineated on the high spatial resolution T_2-weighted images by a radiologist (G.H., 7 years of experience) blinded to patient outcome and DCE-MRI data. To convert ROIs to the spatial resolution of T_1 mapping and dynamic images, ROI masks were downsampled using MRIcro (Version 1.4, Chris Rorden, Columbia, SC, USA; www.mricro.com).

Patient specific arterial input functions were measured from the DCE-MRI images by manually drawing an arterial ROI in the descending aorta. Each arterial ROI was drawn in the dynamic frame showing maximal enhancement, and in a slice distal to inflowing spins to minimise inflow enhancement effects (Roberts *et al*, 2011). Slices near the edge of the field of view were discounted to minimise the influence of transmit B_1 field inhomogeneity. Arterial signal intensity was converted to contrast agent concentration using an assumed pre-contrast T_1 value for blood of 1.2 s (Stark *et al*, 1999) and the SPGR signal equation (Frahm *et al*, 1986). Blood contrast agent concentrations were converted to plasma concentrations using a literature value for haematocrit of 0.42 (Sharma and Kaushal, 2006).

DCE-MRI images were co-registered using a rigid-body model-based approach (Buonaccorsi *et al*, 2007). The 2CXM parameters (plasma flow, F_p (ml min^{-1} ml^{-1}); permeability surface-area product, *PS* (ml min^{-1} ml^{-1}); fractional interstitial volume, v_e (ml ml^{-1}); and fractional plasma volume, v_p (ml ml^{-1}) were estimated at each voxel by jointly fitting T_1 mapping and dynamic signal models (Dickie *et al*, 2015) using the Levenberg-Marquardt least squares algorithm (Marquardt, 1963) in IDL 8.2.2 (Exelis Visual Information Solutions, Boulder, Colorado, USA). The contrast agent volume transfer constant, K^{trans} (min^{-1}), was computed from estimates of F_p and *PS* using the compartment model extraction fraction equation: $K^{trans} = EF_p$, where the first-pass extraction fraction $E = PS/(F_p + PS)$ (Sourbron and Buckley, 2013). For input into survival modelling, voxel-wise 2CXM parameter estimates were summarised using the median.

Clinicopathologic variables. Clinicopathologic characteristics of the cohort are shown in Supplementary Table 1. The following variables were obtained for each patient: primary tumour (T) stage, nodal status, histological subtype, tumour volume, and patient age. Primary tumour stage was assessed using routine T_1 and T_2-weighted MRI scans against the American Joint Committee on

Cancer staging criteria (Greene *et al*, 2002). Involvement of pelvic and/or para-aortic lymph nodes was assessed on large field of view coronal and transverse T_1-weighted and sagittal T_2-weighted imaging. Tumour volumes were computed from the T_2-weighted images by multiplying the number of voxels in the tumour ROI by the voxel volume.

Patient follow-up. Following treatment, patients attended clinic every 3 months in years one and two, and twice per year thereafter, unless symptomatic. Patients underwent clinical examination at each visit. MRI scans (sagittal, transverse, and coronal T_2-weighted turbo spin echo sequences) were used to confirm suspected recurrent disease. If disease was central and amenable to salvage surgery, biopsies were also taken as a definitive marker of recurrence. Treating physicians were blinded to DCE-MRI data.

Survival analysis. The primary endpoint was disease-free survival (DFS). Events were classed as primary, local, or distant disease recurrence or death by any cause. Time to event was calculated from the first fraction of radiotherapy. If an event was not observed before the last recorded follow-up date, the observation was right censored.

Receiver operator characteristic (ROC) analysis was performed to determine the most appropriate cut-off value to dichotomise continuous variables (median DCE-MRI parameters, patient age, and tumour volume). Cut-off values were chosen using the Youden *J* index (Fluss *et al*, 2005) which identifies the cut-off that satisfies *max*(sensitivity–specificity). Cut-offs were limited to the thirtieth to seventieth percentile range to ensure each risk group contained at least 10 patients. If the *J* index lay outside this range the closest percentile within the allowed range was used. T stage was dichotomised as early (T1/T2a) *vs* advanced stage (T2b/T4); histological subtype as squamous cell carcinoma (SCC) *vs* all other subtypes; treatment as chemoradiotherapy *vs* radiotherapy alone; and nodal status as zero *vs* at least one involved node.

For each variable, univariate Cox regression was used to estimate DFS hazard ratios (HRs). *P*-values and 95% confidence intervals (CI) for HRs were computed using a two-tailed Wald test. *P*-values <0.05 were considered statistically significant. Kaplan–Meier survival curves were estimated to allow visual comparison of DFS between risk groups.

The utility of clinicopathologic and DCE-MRI variables for predicting DFS was assessed in a multivariate setting using the random survival forest (RSF) algorithm (Ishwaran *et al*, 2008). The RSF is a non-parametric ensemble tree algorithm that models the effect of multiple (possibly highly correlated) variables on the risk of recurrence/death with minimal assumptions (Ishwaran *et al*, 2008). To determine the relative prognostic value of each variable, accounting for possible confounding and variable interactions, an RSF model was trained using all clinicopathologic and 2CXM variables and the variable importance (VIMP) statistic computed (Ishwaran *et al*, 2008). Broadly speaking, this statistic evaluates how the removal of each variable affects the model prediction error on test data. A high VIMP is associated with a large detrimental effect on model predictions, reflecting high prognostic importance. Bootstrapping was used to calculate point estimates and Bonferroni-corrected 95% CIs on VIMP for each variable.

Two further RSF models were built. A null model containing the six clinicopathologic variables and an alternative model containing the top six clinicopathologic and DCE-MRI variables ranked by median VIMP. Six variables were chosen such that the null and alternative model had the same number of independent variables, facilitating a like-for-like comparison. Predictions of recurrence risk were generated for both null and alternative models in a leave-one-out analysis. The discriminatory accuracy of each model was assessed using Harrell's concordance index (c-index) (Harrell *et al*, 1982) and the null hypothesis of no difference in c-indices was tested using a one-sided paired *t*-test with significance threshold $P<0.05$. The ability of each model to separate left-out patients into distinct risk groupings was evaluated using Cox regression and Kaplan–Meier curve analysis.

Partial plots showing the effect of each variable in the alternative model towards risk of recurrence, adjusted for the effect of all other variables, were generated. All survival analyses were performed in R (Version 3.1, R Foundation for Statistical Computing, Vienna, Austria) using the 'survival', 'survcomp', and 'randomForestSRC' packages.

RESULTS

Median follow-up time in surviving patients was 7.2 years (range 3.2–10.4 years). No patients were lost to follow-up. Table 1 shows results from the ROC analysis including the Youden cut-off values for each continuous variable. Supplementary Figure 2 shows the ROC curves for each continuous variable.

Supplementary Table 2 shows univariate Cox model hazard ratios (HRs) and *P*-values for all variables. Figure 1 shows Kaplan–Meier (KM) DFS curve estimates for variables with hazard ratios that differed significantly from 1 ($P<0.05$). Significant variables were treatment type (HR = 3.9, $P=0.0049$), nodal status (HR = 2.9, $P=0.037$), patient age (HR = 3.9, $P=0.019$), tumour volume (HR = 2.6, $P=0.047$), plasma flow (F_p; HR = 0.25, $P=0.0095$), and contrast agent transfer constant (K^{trans}; HR = 0.20, $P=0.032$). Kaplan–Meier curves for all other variables are shown in Supplementary Figure 3. While non-significant, high *PS*, high v_e, and high v_p were associated with increased DFS. Figure 2 highlights the differences in plasma flow maps for patients with short (0.78–1.1 years) and long (8.4–9.7 years) disease-free

Table 1. Results from ROC analysis applied to continuous variables

	Area under ROC curve	Youden threshold	Threshold percentile	True positives	False positives	True negatives	False negatives	Sensitivity	Specificity
Clinicopathologic									
Patient age	0.74	⩾48 years	⩾47th	14	6	12	4	0.76	0.69
Tumour volume	0.72	⩾99 cm^3	⩾69th	12	8	10	6	0.69	0.64
2CXM									
F_p	0.72	⩾0.32 ml min^{-1} ml^{-1}	⩾50th	13	5	13	5	0.74	0.71
PS	0.65	⩾0.25 ml min^{-1} ml^{-1}	⩾64th	11	7	10	7	0.63	0.59
K^{trans}	0.70	⩾0.12 min^{-1}	⩾69th	11	7	11	7	0.70	0.59
v_p	0.65	⩾0.15 ml ml^{-1}	⩾58th	11	7	11	7	0.63	0.59
v_e	0.61	⩾0.21 ml ml^{-1}	⩾47th	12	6	12	6	0.68	0.65

Abbreviations: F_p = plasma flow; 2CXM = two-compartment exchange model; K^{trans} = contrast agent transfer constant; *PS* = permeability surface-area product; v_p = fractional plasma volume; v_e = fractional interstitial volume; ROC = receiver operator characteristic.

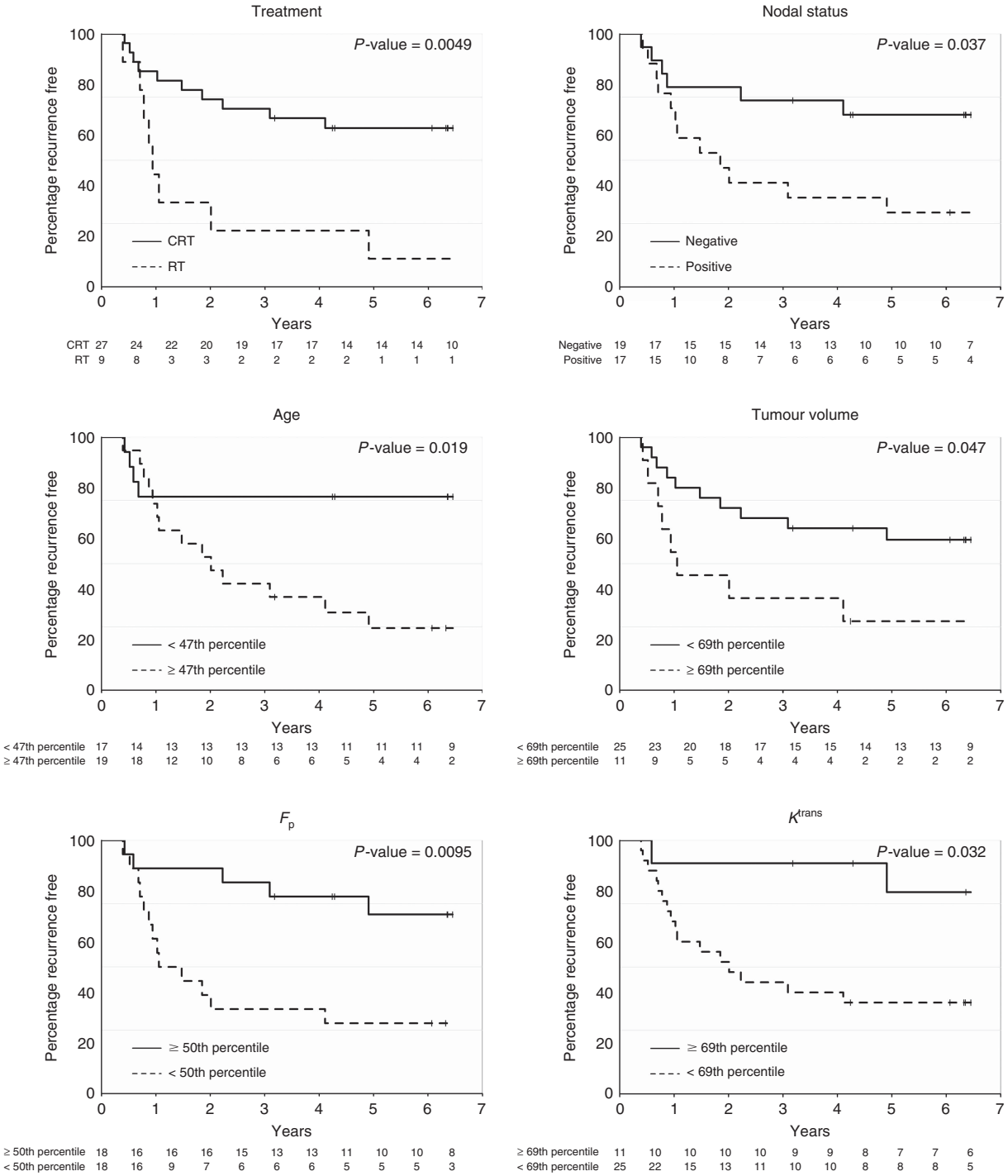

Figure 1. Kaplan–Meier disease-free survival curve estimates for significant variables ($P<0.05$). For the treatment variable, patients were stratified into risk groups based on whether they received radiotherapy alone (RT) or concurrent chemoradiotherapy (CRT). For nodal status, patients were grouped into those with no involved nodes (−ve) or those with at least one involved node (+ve). For patient age, tumour volume, plasma flow, and K^{trans}, patients were stratified into risk groups based on ROC analysis cut-off values.

survival. Differences in K^{trans} maps were not as pronounced as for F_p maps, reflecting a reduction in prognostic ability. *PS* maps appear very similar between short and long DFS groups reflecting low prognostic value.

Results from multivariate random survival forest analyses are shown in Table 2, Figure 3 and 4. Table 2 shows point estimates and 95% confidence intervals on median VIMP. The six most important prognostic variables in order of decreasing VIMP (and those selected for the alternative model) were: plasma flow (F_p), treatment, histological subtype, nodal status, patient age, and the transfer constant K^{trans}. In leave-one-out analysis, the alternative model made statistically significantly more accurate predictions than the null model (c-indices of 0.70 *vs* 0.61, $P=0.0089$). The alternative model was also better at assigning left-out patients into distinct risk groups ($P=0.029$ *vs* $P=0.056$).

Figure 4 shows the prognostic effect of each variable in the alternative model after adjusting for the effect of all other variables in the model. Predicted risks differed significantly between the levels of all variables except for patient age and nodal status (see figure for *P*-values).

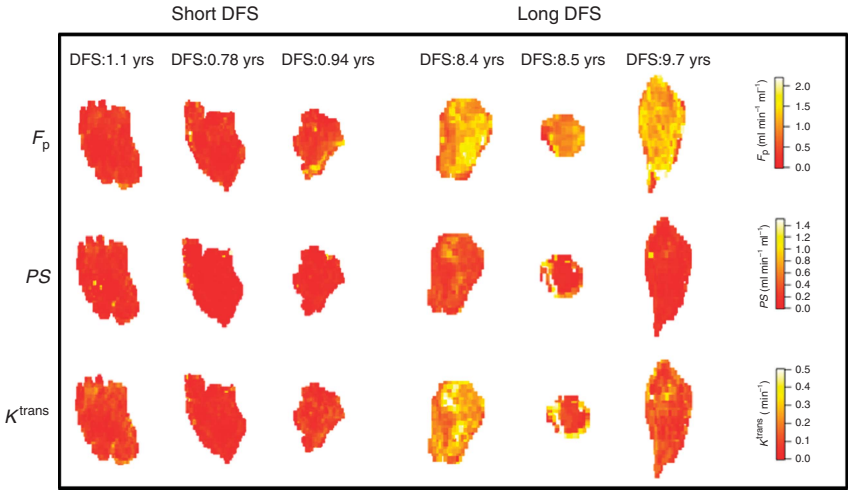

Figure 2. Maps of plasma flow (F_p), permeability surface area product (*PS*), and contrast agent transfer constant (K^{trans}) for representative patients with short (left, DFS = 0.78–1.1 years) and long (right, DFS = 8.4–9.7 years) disease-free survival. A single representative slice is shown for each tumour.

Table 2. Bootstrapped point estimates and Bonferroni-corrected 95% confidence intervals for median variable importance (VIMP)

	Median VIMP (95% CIs)	Rank
Clinicopathologic		
T stage[a]	0.0046 (0.0030, 0.0087)	11
Treatment[b]	**0.044 (0.035, 0.057)**	**2**
Nodal Status[c]	**0.026 (0.018, 0.037)**	**4**
Histological subtype[d]	**0.034 (0.021, 0.049)**	**3**
Patient age	**0.023 (0.018, 0.029)**	**5**
Tumour volume	0.0093 (0.0068, 0.013)	8
2CXM		
F_P	**0.050 (0.039, 0.061)**	**1**
PS	0.0084 (0.0064, 0.011)	9
K^{trans}	**0.019 (0.014, 0.025)**	**6**
v_p	0.018 (0.016, 0.023)	7
v_e	0.0077 (0.0061, 0.0096)	10

Abbreviations: CIs = confidence intervals; 2CXM = two-compartment exchange model; K^{trans} = contrast agent transfer constant; F_p = plasma flow; *PS* = permeability surface-area product; v_p = fractional plasma volume; v_e = fractional interstitial volume. Higher VIMP indicates greater prognostic importance (lower rank). The top 6 variables (boldface) were used to build the alternative model.
[a]T2b/T4 *vs* T1/T2a.
[b]Radiotherapy *vs* chemoradiotherapy.
[c]At least one involved node *vs* no involved nodes.
[d]Other subtypes *vs* squamous cell.

DISCUSSION

Plasma flow (F_p) and the contrast agent transfer constant (K^{trans}) were the only microvascular parameters statistically significantly associated with survival. All other microvascular parameters, including *PS*, showed non-significant ability to stratify patients into distinct risk groupings. In both univariate and multivariate analyses, F_p was shown to be a better predictor of DFS than K^{trans}. These results support the hypothesis that K^{trans} derives its prognostic value from its dependence on F_p but is less useful as a prognostic biomarker, due to its dependence on *PS*.

Other work evaluating the prognostic value of plasma or blood flow in tumours has found confirmatory results. Using DCE-computed tomography in 108 head and neck cancer patients treated with radiotherapy, Hermans *et al* showed high blood flow was associated with reduced risk of local recurrence (Hermans *et al*, 2003). Haldorsen *et al* investigated the prognostic value of DCE-MRI blood flow measurements in patients with endometrial cancer treated with surgery. While not related to response of tumours to chemoradiotherapy, low blood flow was associated with increased expression of microvascular proliferation markers and shorter survival times (Haldorsen *et al*, 2014).

All clinicopathologic factors displayed the expected prognostic trend (Rose *et al*, 1999; Kang *et al*, 2012; Chen *et al*, 2015). Treatment type was one of the strongest prognostic factors in both univariate and multivariate analyses, possibly reflecting the added cytotoxic effect of combined chemoradiotherapy (Rose *et al*, 1999), or a relationship between a patient's ability to tolerate chemotherapy and their subsequent survival. Nodal status and patient age were significant factors in univariate analyses but lost significance when adjusting for other factors (alternative model, Figure 4). Stratification of patients by T stage was not a significant prognostic factor in either univariate or multivariate methods. This was probably due to the small number of patients in the early stage group (T1–T2a) leading to low precision in the estimated hazard ratio.

Biological interpretation. Previous studies across a range of tumour types have shown uptake of MRI contrast agent is associated with the degree of tumour hypoxia. In a melanoma xenograft model, Egeland *et al* showed a strong relationship between pimonidazole stain fraction and K^{trans} (Egeland *et al*, 2012). Halle *et al* observed a negative correlation between maximum amplitude of signal enhancement and HIF-α expression in cervix tumours (Halle *et al*, 2012). Similarly, three cervix cancer studies have shown a strong correlation between tumour oxygen pressure measurements made using polarographic electrodes and maximum relative signal enhancement (Cooper *et al*, 2000; Lyng *et al*, 2001; Loncaster *et al*, 2002). These relationships have subsequently been upheld for more recent measurements of blood flow in cervix and head and neck cancers (Haider *et al*, 2005; Donaldson *et al*, 2011).

Since vessel walls pose little barrier to oxygen (Michel, 1996), *PS* of vessels measured using Gd-DTPA is unlikely to be a good biomarker of tissue oxygenation, unless large differences in vessel surface area are present between tumours. The degree of tissue hypoxia is likely to be more dependent on the supply of oxygen to the capillary bed (i.e., via plasma flow). This may explain why reported correlations between *PS* and tissue oxygenation/hypoxia are weaker than those for F_p (Haider *et al*, 2005; Donaldson *et al*, 2011). Survival analyses presented in this study support the hypothesis that plasma flow could be a more sensitive measure of

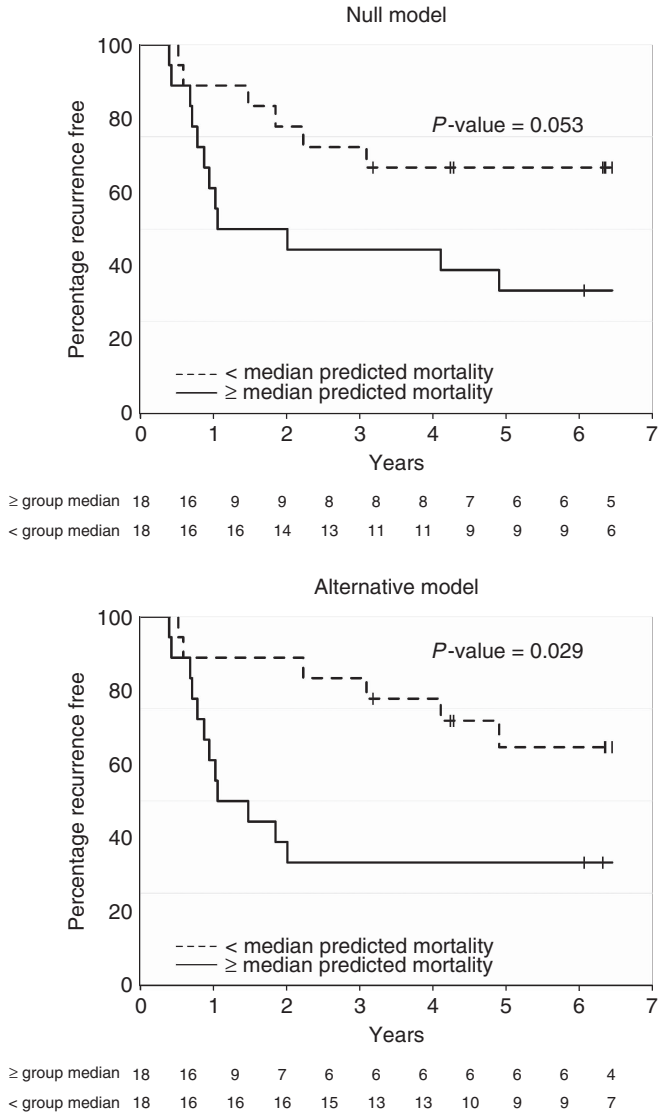

Figure 3. Kaplan–Meier disease-free survival curve estimates for low and high-risk patients as predicted by the null (top) and alternative (bottom) models. Predictions of recurrence risk were estimated for each patient using the random survival forest algorithm in a leave-one-patient-out analysis. Patients were then grouped into low and high risk groups based on the median predicted recurrence/death risk. *P*-values show the result of testing the null hypothesis that HR = 1.

tissue oxygenation compared with K^{trans} and *PS*, however further work is needed to definitively test this hypothesis.

In this study, measurements of *PS* represent the leakiness of vessels to Gd-DTPA and will approximate the permeability of vessels to molecules of similar size (i.e., such as cisplatin). The prognostic trend of *PS* observed could reflect sensitivity to differences in chemotherapy drug delivery for those patients treated with chemoradiotherapy. Under this reasoning, the observed lack of statistical significance for *PS* could be due to inclusion of nine patients in the sample who received only radiotherapy and would therefore not be affected by *PS*. Alternatively, the difference in *PS* between patients may not be sufficient to cause a meaningful difference in the delivery rate of chemotherapy to tumour cells. Delivery of chemotherapy may be rate limited by other factors such as the metabolism rate of the chemotherapy agent or diffusion rate across the extravascular space (Minchinton and Tannock, 2006).

The weak relationship between v_e and DFS could reflect reduced tumour cell density ($v_{cell} \sim 1 - v_b - v_e$, where v_{cell} is the volume fraction of tumour cells). Plasma volume fraction was not prognostic despite a positive correlation with F_p (Pearson $r = 0.6$, data not shown). Simulation data from Luypaert *et al* (2010) suggests 2CXM estimates of v_p are less precise than F_p, which would explain reduced prognostic ability if effects of F_p and v_p on survival are similar.

Study limitations. While prospective, the number of patients analysed ($n = 36$) relative to the number of independent variables ($p = 11$) was small. Classical multivariate statistical methods such as Cox proportional hazards modelling are unsuitable for such analyses. Low n/p gives rise to high variance in estimated model coefficients, leading to high-generalisation error (Harrell *et al*, 1996). An obvious solution is to recruit more patients, but that approach has strong ethical, economic, and practical disincentives. To address this issue, we used a state-of-the-art survival model called the random survival forest (RSF). The RSF is an ensemble model that develops on bootstrap aggregation (Breiman, 1996, 2001) and random variable selection (Ho, 1998) to model right-censored survival data. The model makes very few assumptions about the data (notably it does not depend on the proportional hazards assumption of the Cox model). It also facilitates reliable and objective automatic variable selection in the p ≈ n regime, as demonstrated by (Ishwaran *et al*, 2008).

There was heterogeneity in the treatment patients received. To control for possible confounding (Rose *et al*, 1999; Nag *et al*, 2000), a treatment variable was included in the multivariate models to adjust for the presence or absence of chemotherapy amongst patients. Given the small sample size, adjustment for the presence or absence of brachytherapy or external beam boosts was not made.

Future work. The results of this study should be validated in an independent cohort and test-retest reproducibility of DCE-MRI F_p measurements assessed (O'Connor *et al*, 2016). Further work should also aim to correlate DCE-MRI F_p measurements with *in-vivo* Eppendorf electrode pO_2 measurements and determine the extent to which F_p can be used as a biomarker of tumour oxygenation. Alternatively, development and validation of perfusion measurements using more readily available technologies such as contrast-enhanced (microbubble) transvaginal ultrasound may lead to cheaper and faster translation to the clinic.

Ultimately, pre-treatment blood flow measurements may be useful to identify patients suitable for treatment modifications such as dose escalation, use of hypoxia-modifying treatments such as accelerated radiotherapy with carbogen and nicotinimide (ARCON (Bernier *et al*, 2000)), or pre-radiotherapy vascular normalisation using anti-angiogenic agents such as bevacizumab (Tewari *et al*, 2014).

CONCLUSIONS

The prognostic value of contrast agent uptake observed in cervical cancer patients treated with chemoradiotherapy can be attributed mainly to contributions from plasma flow (F_p) rather than permeability surface-area product (*PS*). Plasma flow may better reflect tumour oxygenation and thus provide more specific information on radiotherapy efficacy. Future work should focus on the qualification and validation of F_p as a prognostic biomarker in cervical cancer, in particular the development and validation of low cost methods to facilitate rapid translation into the clinic.

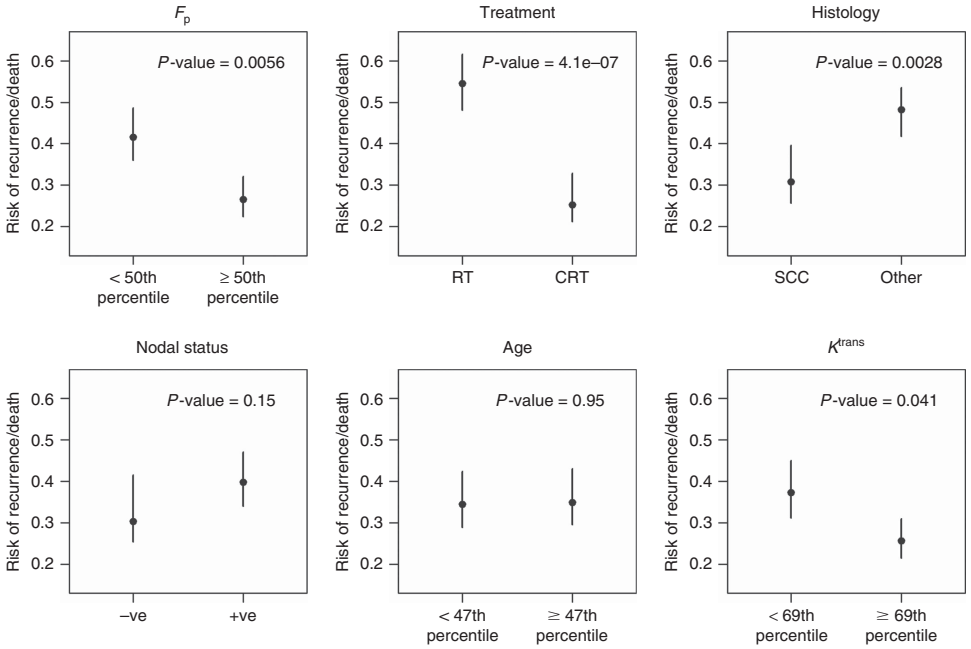

Figure 4. Random survival model predictions of recurrence risk for each variable in the alternative model. Probabilities are adjusted for the effect of all other variables in the model. Variables are ordered from top-left (strongest predictor) to bottom-right (weakest predictor) by median VIMP. Dots show point estimates on median recurrence risk. Lines extend to ~95% confidence intervals. *P*-values show the result of testing the null hypothesis of no difference in predicted recurrence risk between levels of each factor.

ACKNOWLEDGEMENTS

We would like to thank Professor David Buckley for discussions regarding the manuscript. The work was supported by the Christie Hospital NHS Foundation Trust.

CONFLICT OF INTEREST

The authors declare no conflict of interest.

REFERENCES

Andersen EKF, Hole K, Lund KV, Sundfør K, Kristensen GB, Lyng H, Malinen E (2013) Pharmacokinetic parameters derived from dynamic contrast enhanced MRI of cervical cancers predict chemoradiotherapy outcome. *Radiother Oncol* **107**: 117–122.

Bernier J, Denekamp J, Rojas A, Minatel E, Horiot J, Hamers H, Antognoni P, Dahl O, Richaud P, van Glabbeke M, Piérart M (2000) ARCON: accelerated radiotherapy with carbogen and nicotinamide in head and neck squamous cell carcinomas. The experience of the Co-operative group of radiotherapy of the european organization for research and treatment of cancer (EORTC). *Radiother Oncol* **55**: 111–119.

Breiman L (1996) Bagging predictors. *Mach Learn* **24**: 123–140.

Breiman L (2001) Random forests. *Mach Learn* **45**: 5–32.

Brix G, Kiessling F, Lucht R, Darai S, Wasser K, Delorme S, Griebel J (2004) Microcirculation and microvasculature in breast tumors: pharmacokinetic analysis of dynamic MR image series. *Magn Reson Med* **52**: 420–429.

Buonaccorsi GA, O'Connor JP, Caunce A, Roberts C, Cheung S, Watson Y, Davies K, Hope L, Jackson A, Jayson GC, Parker GJ (2007) Tracer kinetic model–driven registration for dynamic contrast-enhanced MRI time-series data. *Magn Reson Med* **58**: 1010–1019.

Chen C, Wang L, Lin J, Jan J (2015) The prognostic factors for locally advanced cervical cancer patients treated by intensity-modulated radiation therapy with concurrent chemotherapy. *J Formos Med Assoc* **114**: 231–237.

Cooper R, Carrington BM, Loncaster J, Todd SM, Davidson SE, Logue JP, Luthra AD, Jones AP, Stratford I, Hunter RD, West CM (2000) Tumour oxygenation levels correlate with dynamic contrast-enhanced magnetic resonance imaging parameters in carcinoma of the cervix. *Radiother Oncol* **57**: 53–59.

Dickie B (2017) MRdep/Predicting-Survival-in-Cervical-Cancer-using-DCE-MRI: Predicting-Survival-in-Cervical-Cancer-using-DCE-MRI: Software and Data for Survival Analysis in Patients with Locally Advanced Cervical Cancer_v3 [Data set]. *Zenodo* doi:10.5281/zenodo.1495211.

Dickie BR, Banerji A, Kershaw LE, Mcpartlin A, Choudhury A, West CM, Rose CJ (2015) Improved accuracy and precision of tracer kinetic parameters by joint fitting to variable flip angle and dynamic contrast enhanced MRI data. *Magn Reson Med* **76**: 1270–1281.

Donaldson SB, Betts G, Bonington SC, Homer JJ, Slevin NJ, Kershaw LE, Valentine H, West CM, Buckley DL (2011) Perfusion estimated with rapid dynamic contrast-enhanced magnetic resonance imaging correlates inversely with vascular endothelial growth factor expression and pimonidazole staining in head-and-neck cancer: a pilot study. *Int J Radiat Oncol Biol Phys* **81**: 1176–1183.

Donaldson SB, West CML, Davidson SE, Carrington BM, Hutchison G, Jones AP, Sourbron SP, Buckley DL (2010) A comparison of tracer kinetic models for T1-weighted dynamic contrast-enhanced MRI: application in carcinoma of the cervix. *Magn Reson Med* **63**: 691–700.

Egeland TAM, Gulliksrud K, Gaustad J, Mathiesen B, Rofstad EK (2012) Dynamic Contrast-Enhanced-MRI of Tumor Hypoxia. *Magn Reson Med* **67**: 519–530.

Fluss R, Faraggi D, Reiser B (2005) Estimation of the Youden Index and its Associated Cutoff Point. *Biom J* **47**: 458–472.

Frahm J, Haase A, Matthaei D (1986) Rapid three-dimensional MR imaging using the FLASH technique. *J Comput Assist Tomogr* **10**: 363–368.

Greene, Frederick L, David LP, Irvin DF, April GF, Charles MB, Daniel GH, Monica M (2002) *AJCC Cancer Staging Manual,* Volume 1. (Springer Science & Business Media). 6th ed. Springer-Verlag: New York, NY, USA.

Haider MA, Milosevic M, Fyles A, Sitartchouk I, Yeung I, Henderson E, Lockwood G, Lee TY, Roberts TP (2005) Assessment of the tumor microenvironment in cervix cancer using dynamic contrast enhanced CT, interstitial fluid pressure and oxygen measurements. *Int J Radiat Oncol Biol Phys* **62**: 1100–1107.

Haldorsen IS, Stefansson I, Grüner R, Husby JA, Magnussen IJ, Werner HMJ, Salvesen ØO, Bjørge L, Trovik J, Taxt T, Akslen LA, Salvesen HB (2014) Increased microvascular proliferation is negatively correlated to tumour blood flow and is associated with unfavourable outcome in endometrial carcinomas. *Br J Cancer* **110**: 107–114.

Halle C, Andersen E, Lando M, Aarnes E, Hasvold G, Holden M, Syljua RG, Sundfør K, Kristensen GB, Holm R, Malinen E, Lyng H (2012) Hypoxia-induced gene expression in chemoradioresistant cervical cancer revealed by dynamic contrast-enhanced MRI. *Cancer Res* **72**(20): 5285–5295.

Harrell FE, Califf RM, Pryor DB, Lee KL, Rosati RA (1982) Evaluating the yield of medical tests. *J Am Med Assoc* **247**: 2543–2546.

Harrell FE, Lee KL, Mark DB (1996) Multivariable prognostic models: issues in developing models, evaluating assumptions and adequacy, and measuring and reducing errors. *Stat Med* **15**: 361–387.

Hermans R, Meijerink M, Van Den Bogaert W, Rijnders A, Weltens C, Lambin P (2003) Tumor perfusion rate determined noninvasively by dynamic computed tomography predicts outcome in head-and-neck cancer after radiotherapy. *Int J Radiat Oncol Biol Phys* **57**: 1351–1356.

Ho TK (1998) The random subspace method for constructing decision forests. *Pattern Anal Mach Intell IEEE Trans* **20**: 832–844.

Ishwaran H, Kogalur UB, Blackstone EH, Lauer MS (2008) Random survival forests. *Ann Appl Stat* **2**: 841–860.

Kang S, Nam B-H, Park J-Y, Seo S-S, Ryu S-Y, Kim JW, Kim S-C, Park S-Y, Nam J-H (2012) Risk assessment tool for distant recurrence after platinum-based concurrent chemoradiation in patients with locally advanced cervical cancer: a Korean gynecologic oncology group study. *J Clin Oncol* **30**: 2369–2374.

Loncaster JA, Carrington BM, Sykes JR, Jones AP, Todd SM, Cooper R, Buckley DL, Davidson SE, Logue JP, Hunter RD, West CML (2002) Prediction of radiotherapy outcome using dynamic contrast enhanced MRI of carcinoma of the cervix. *Int J Radiat Oncol Biol Phys* **54**: 759–767.

Luypaert R, Ingrisch M, Sourbron S, Gill AB, Black RT, Bowden DJ (2010) Error estimation for perfusion parameters obtained using the two-compartment exchange model in dynamic contrast-enhanced MRI: a simulation study. *Phys Med Biol* **55**: 6431–6443.

Lyng H, Vorren AO, Sundfør K, Taksdal I, Lien HH, Kaalhus O, Rofstad EK (2001) Assessment of tumor oxygenation in human cervical carcinoma by use of dynamic gd-dtpa- enhanced mr imaging. *J Magn Reson Imaging* **14**: 750–756.

Marquardt DW (1963) An algorithm for least-squares estimation of nonlinear parameters. *J Soc Ind Appl Math* **11**: 431–441.

Mayr NA, Yuh WT, Magnotta VA, Ehrhardt JC, Wheeler JA, Sorosky JI, Davis CS, Wen BC, Martin DD, Pelsang RE, Buller RE, Oberley LW, Mellenberg DE, Hussey DH (1996) Tumor perfusion studies using fast magnetic resonance imaging technique in advanced cervical cancer: a new noninvasive predictive assay. *Int J Radiat Oncol Biol Phys* **36**: 623–633.

Mayr NA, Yuh WTC, Jajoura D, Wang JZ, Lo SS, Montebello JF, Porter K, Zhang D, McMeekin DS, Buatti JM (2010) Ultra-early predictive assay for treatment failure using functional magnetic resonance imaging and clinical prognostic parameters in cervical cancer. *Cancer* **116**: 903–912.

Michel CC (1996) Transport of macromolecules through microvascular walls. *Cardiovasc Res* **32**: 644–653.

Minchinton AI, Tannock IF (2006) Drug penetration in solid tumours. *Nat Rev Cancer* **6**: 583–592.

Moher D, Schulz KF, Altman DG (2001) The CONSORT statement: revised recommendations for improving the quality of reports of parallel-group randomised trials. *Lancet* **357**: 1191–1194.

Nag S, Erickson B, Thomadsen B, Orton C, Demanes JD, Petereit D (2000) The American Brachytherapy Society recommendations for high-dose-rate brachytherapy for carcinoma of the cervix. *Int J Radiat Oncol Biol Phys* **48**: 201–211.

O'Connor JPB, Aboagye EO, Adams JE, Aerts HJWL, Barrington, Sally F, Beer AJ, Boellaard R, Bohndiek SE, Brown G, Brady M, Buckley DL, Chenevert TL, Clarke LP, Collette S, Cook GJ, DeSouza NM, Dickson JC, Dive C, Evelhoch JL, Faivre-Finn C, Gallagher FA, Gilbert FJ, Gillies RJ, Goh V, Griffiths JR, Groves AM, Halligan S, Harris AL, Hawkes DJ, Hoekstra OS, Huang EP, Hutton BF, Jackson EF, Jayson GC, Jones A, Koh D, Lacombe D, Lambin P, Lassau N, Leach MO, Lee T-Y, Leen EL, Lewis JS, Liu Y, Lythgoe MF, Manoharan P, Maxwell RJ, Miles KA, Morgan B, Morris S, Ng T, Padhani AR, Parker GJ, Partridge M, Pathak AP, Peet AC, Punwani S, Reynolds AR, Robinson SP, Shankar LK, Sharma RA, Soloviev D, Stroobants S, Sullivan DC, Taylor SA, Tofts PS, Tozer GM, van Herk M, Walker-Samuel S, Wason J, Williams KJ, Workman P, Yankeelov T, Brindle KM, McShane LM, Jackson A, Waterton JC (2016) Imaging Biomarker Roadmap for Cancer Studies. *Nat Rev Clin Oncol* **14**(3): 169–186.

Roberts C, Little R, Watson Y, Zhao S, Buckley DL, Parker GJM (2011) The effect of blood inflow and B(1)-field inhomogeneity on measurement of the arterial input function in axial 3D spoiled gradient echo dynamic contrast-enhanced MRI. *Magn Reson Med* **65**: 108–119.

Rose PG, Bundy BN, Watkins EB, Thigpen JT, Deppe G, Maiman MA, Clarke-Pearson DL, Insalaco S (1999) Concurrent cisplatin-based radiotherapy and chemotherapy for locally advanced cervical cancer. *N Engl J Med* **340**: 1144–1153.

Semple SIK, Harry VN, Parkin DE, Gilbert FJ (2009) A combined pharmacokinetic and radiologic assessment of dynamic contrast-enhanced magnetic resonance imaging predicts response to chemoradiation in locally advanced cervical cancer. *Int J Radiat Oncol Biol Phys* **75**: 611–617.

Sharma S, Kaushal R (2006) *Rapid Review of Clinical Medicine for MRCP Part 2*. CRC Press: London.

Sourbron SP, Buckley DL (2011) On the scope and interpretation of the Tofts models for DCE-MRI. *Magn Reson Med* **66**: 735–745.

Sourbron SP, Buckley DL (2013) Classic models for dynamic contrast-enhanced MRI. *NMR Biomed* **26**: 1004–1027.

St Lawrence KS, Lee TY (1998) An adiabatic approximation to the tissue homogeneity model for water exchange in the brain: I. Theoretical derivation. *J Cereb Blood Flow Metab* **18**: 1365–1377.

Stark DD, Bradley WG (1999) *Magnetic Resonance Imaging*. Philadelphia: Mosby.

Stollberger R, Fazekas F (2004) Improved perfusion and tracer kinetic imaging using parallel imaging. *Top Magn Reson Imaging* **15**: 245–255.

Tewari KS, Sill MW, Long HJ, Penson RT, Huang H, Ramondetta LM, Landrum LM, Oaknin A, Reid TJ, Leitao MM, Michael HE, Monk BJ (2014) Improved survival with bevacizumab in advanced cervical cancer. *N Engl J Med* **370**: 734–743.

Tofts PS, Brix G, Buckley DL, L Evelhoch J, Henderson E, Knopp MV, Larsson HBW, Lee T-Y, Mayr NA, Parker GJM, Port RE, Taylor J, Weisskoff RM (1999) Estimating kinetic parameters from dynamic contrast-enhanced T1-weighted\tMRI of a diffusable tracer: standardized quantities and symbols. *J Magn Reson Imaging* **10**: 223–232.

Yuh WTC, Mayr NA, Jarjoura D, Wu D, Grecula JC, Lo SS, Edwards SM, Magnotta VA, Sammet S, Zhang H, Montebello JF, Fowler J, Knopp MV, Wang JZ (2009) Predicting control of primary tumor and survival by DCE MRI during early therapy in cervical cancer. *Invest Radiol* **44**: 343–350.

Zahra MA, Tan LT, Priest AN, Graves MJ, Arends M, Crawford RA, Brenton JD, Lomas DJ, Sala E (2009) Semiquantitative and quantitative dynamic contrast-enhanced magnetic resonance imaging measurements predict radiation response in cervix cancer. *Int J Radiat Oncol Biol Phys* **74**: 766–773.

Supplementary Information accompanies this paper on British Journal of Cancer website (http://www.nature.com/bjc)